7. S. Mann, *Nature* **365**, 499 (1993).
8. E. Dujardin, S. Mann, *Adv. Eng. Mater.* **4**, 461 (2002).
9. L. Addadi, S. Weiner, *Angew. Chem. Int. Ed. Engl.* **31**, 153 (1992).
10. S. Weiner, L. Addadi, *J. Mater. Chem.* **7**, 689 (1997).
11. Y.-J. Lee, J. S. Lee, Y. S. Park, K. B. Yoon, *Adv. Mater.* **13**, 1259 (2001).
12. Materials and methods are available as supporting material on *Science* Online.
13. D. L. Pavia, G. M. Lampman, G. S. Kriz, *Introduction to Spectroscopy* (Saunders College Publishing, Orlando, FL, 1996).
14. M. M. J. Treacy, J. B. Higgins, *Collection of Simulated XRD Powder Patterns for Zeolites* (Elsevier, Amsterdam, 2001).
15. The simulated relative intensities of the (101), (200), (002), and (102) reflections of the randomly oriented powders are 68.4, 31.3, 6.8, and 17.4, respectively (*13*). The reflection multiplicities and structure factors were taken into account during simulation of the relative intensities.
16. C. E. A. Kirschhock, R. Ravishankar, P. A. Jacobs, J. A. Martens, *J. Phys. Chem.* **103**, 11021 (1999).
17. C. E. A. Kirschhock, S. P. B. Kremer, P. J. Grobet, P. A. Jacobs, J. A. Martens, *J. Phys. Chem.* **106**, 4897 (2002).
18. J. H. Koegler, H. van Bekkum, J. C. Jansen, *Zeolites* **19**, 262 (1997).
19. J. Caro *et al.*, *Adv. Mater.* **4**, 273 (1992).
20. S. Feng, T. Bein, *Nature* **368**, 834 (1994).
21. S. Feng, T. Bein, *Science* **265**, 1839 (1994).
22. G. Calzaferri *et al.*, *J. Mater. Chem.* **12**, 1 (2002).
23. U. Vietze *et al.*, *Phys. Rev. Lett.* **81**, 4628 (1998).
24. We thank the Ministry of Science and Technology of Korea for supporting this work through the Creative Research Initiatives program.

Supporting Online Material
www.sciencemag.org/cgi/content/full/301/5634/818/DC1
Materials and Methods
Figs. S1 to S9

5 May 2003; accepted 25 June 2003

Thermohaline Fine Structure in an Oceanographic Front from Seismic Reflection Profiling

W. Steven Holbrook,[1]* Pedro Páramo,[1] Scott Pearse,[1] Raymond W. Schmitt[2]

We present acoustic images of oceanic thermohaline structure created from marine seismic reflection profiles across the major oceanographic front between the Labrador Current and the North Atlantic Current. The images show that distinct water masses can be mapped, and their internal structure imaged, using low-frequency acoustic reflections from sound speed contrasts at interfaces across which temperature changes. The warm/cold front is characterized by east-dipping reflections generated by thermohaline intrusions in the uppermost 1000 meters of the ocean. Our results imply that marine seismic reflection techniques can provide excellent spatial resolution of important oceanic phenomena, including thermohaline intrusions, internal waves, and eddies.

Many parts of the world's oceans contain layers with contrasting temperature and salinity that produce fine-scale thermohaline structure (*1, 2*), such as thermohaline staircases (*3*), which occur in tropical and subtropical regions, and lateral intrusions, which are common at fronts between major water masses (*4, 5*). These structures are important manifestations of mixing processes in the ocean. Thermohaline fine structure is commonly mapped by instruments that measure depth profiles of temperature and salinity, either at single locations or by towed vehicles that fly a "tow-yo" or sawtooth pattern (*6, 7*). Such techniques have practical limitations in the volume of ocean that can be sampled and in the horizontal resolution that can be achieved. Here, we present evidence that thermohaline structure in the ocean can be imaged over large areas and full ocean depth, with high lateral resolution, using standard marine seismic reflection techniques. To our knowledge, such low-frequency (10 to 100 Hz) water column reflections have been reported only rarely (*8, 9*) and have not previously been linked to fine-scale thermohaline structure. Although high-frequency (100 kHz to 1 MHz) scattering from upper ocean microstructure or zooplankton is often used to image upper ocean internal waves (*10, 11*), it is not capable of imaging to abyssal depths and has rather different backscattering mechanisms because of the much shorter acoustic wavelengths.

We observed seismic reflections from the water column on data acquired in August 2000 by R/V *Maurice Ewing* on three long transects that directly cross the climatological path of the North Atlantic Current (NAC) (Fig. 1). Analysis of shot and common-midpoint (CMP) gathers unequivocally shows that the energy represents primary reflections rather than multiples, refractions, or diffractions: Reflections are visible at zero offset, show hyperbolic move-out, asymptotically approach the direct water wave, and are consistent from shot to shot (*12*). Stacks of these reflections by conventional methods—including velocity analysis, filtering, and median stacking—show striking images of reflectance in the water column (Figs. 2 to 4) (*13*). Clear, coherent reflections are present on all three transects, especially in the upper 1.5 s of two-way travel time (~1100 m depth). The recording geometry provided stacked traces at a lateral spacing of 6.25 m (*14*). Sea surface temperature (SST) measurements acquired during seismic profiling show the front between the Labrador Current (LC) and the NAC and show that seismic reflectance differs between these water masses.

The impedance contrasts responsible for the observed reflections are caused by small changes in sound speed between distinct layers, likely thermohaline intrusions. Two hydrographic data sets support this notion. First, previous oceanographic studies in this immediate region (*15, 16*) show exceptionally strong intrusions between the NAC and LC, very near the site of strong reflections in our data. Second, an expendable bathythermograph (XBT) acquired during our cruise recorded strong temperature inversions (up to 5°C) in a location on one of our seismic lines (Fig. 5). Assuming a reasonable temperature-salinity relationship consistent with static stability and the usual properties of such intrusions, we generated a plausible salinity profile for this XBT and then used the temperature and salinity profiles to calculate sound speed and density, with temperature having the dominant influence. The strong temperature anomalies predict substantial vertical variations in sound speed in the uppermost 400 m of the ocean (Fig. 5). Density is predicted to show only small contrasts, because temperature and salinity typically covary so as to compensate density in such thermohaline intrusions (*7*).

Comparison of the predicted sound speed profile and the coincident stacked seismic reflection data shows a remarkable match (Fig. 5). The reflective upper 0.5 s of the section corresponds exactly with the portion of the sound speed profile that shows fine-scale structure, and several individual reflections can be correlated precisely to corresponding jumps in sound speed. For example, the strong reflection at 0.32 s has a measured reflection coefficient of −0.005 (*17, 18*), which is exactly the expected value for the observed sound speed decrease of 15 m/s if density is constant across the interface (Fig. 5). The weaker reflection at 0.5 s has a reflection coefficient of 0.0007, corresponding

[1]Department of Geology and Geophysics, University of Wyoming, Laramie, WY 82071, USA. [2]Department of Physical Oceanography, Woods Hole Oceanographic Institution, Woods Hole, MA 02543, USA.

*To whom correspondence should be addressed. E-mail: steveh@uwyo.edu

to a sound speed change of 2 m/s. The sound speed changes of 15 m/s and 2 m/s are caused by temperature changes of 3°C and 0.4°C, respectively, as measured by the XBT. Deeper, weaker reflections observed on the seismic sections indicate that reflections can be imaged from boundaries with reflection coefficients as low as 0.0001, corresponding to sound speed changes of 0.3 m/s (temperature changes of ~0.1°C). The ability to detect returns from such weak boundaries is due to the strong 20-gun sound source, the relatively quiet recording conditions, and the low-loss acoustic medium (water) through which the seismic waves propagated. Wavelengths in our data range from 15 to 75 m, implying that layers as thin as ~4 m are detectable; intrusions in the study area are typically tens of meters thick (Fig. 5).

Our images show the two-dimensional fine-scale thermohaline structure of the ocean in great detail. We observe at least four styles of reflectance in the uppermost 1000 m, which we discuss below: (i) weak, subhorizontal, discontinuous reflections; (ii) wedges of strong, east-dipping reflections near the front; (iii) long, continuous reflections in the uppermost ~500 m that are either horizontal or dip gently (<0.5°) either westward or (usually) eastward; and (iv) coherent, reflective slabs, surrounded by transparent regions, that dip at 1° to 5°.

In the warm waters of the NAC, near-horizontal reflections are common. These events are typically 0.5 to 5 km long, have reflection coefficients of 0.0002 (which would be produced by sound speed contrasts of ~0.6 m/s or density contrasts of 0.4 kg/m^3), and occupy the uppermost 750 m of the ocean. The near-horizontal orientation of these reflections matches the weak tilt of lateral intrusions observed previously in the NAC (*15*). Intrusions show a weak tilt across isopycnal surfaces as a result of double-diffusive mixing (*14*), whereas the isopycnal surfaces tilt more strongly across a front such as the NAC as a result of the geostrophic dynamical balance. The weakening of reflectance at 750 m depth represents the base of the thermocline. In places, reflections within the NAC show slight undulations, with horizontal wavelengths of about 700 m and peak-to-trough amplitudes of ~10 m. We interpret these undulations to be internal waves, which often have dimensions on this order in the upper ocean (*19*). Similar undulations are imaged elsewhere on the profile (*20*).

Wedges of strong, east-dipping reflections dominate the frontal boundary, where SSTs increase from about 16° to 20°C. Fronts between warm-salty and cold-fresh water masses are typically sites of strong thermohaline

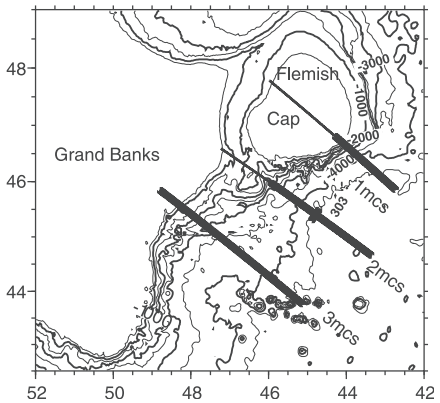

Fig. 1. Location of seismic lines in the Newfoundland Basin. Bold lines show portions of seismic lines shown in Figs. 2 to 5.

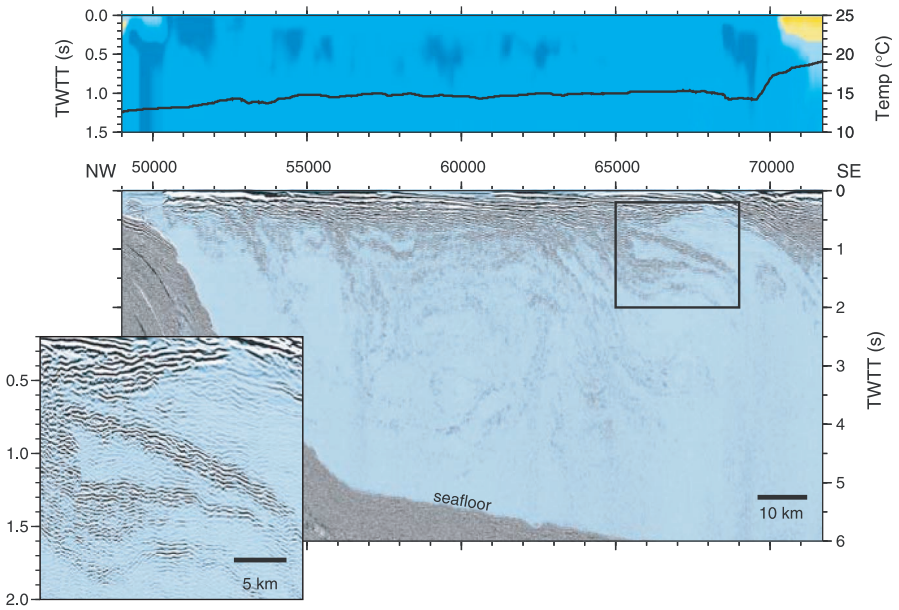

Fig. 2. Bottom: Stacked seismic section of water column on Line 1mcs. Image has a vertical exaggeration of 16. Vertical axis is two-way travel time (TWTT) in seconds; the base of the section at 6 s corresponds to a depth of ~4500 m in the ocean. Horizontal axis is in CMP; CMP spacing is 6.25 m. Box denotes portion of profile depicted in inset, which shows coherent "slabs" penetrating to ~1000 m depth. Top: Color-coded plot of stacking sound speed in the ocean, which is approximately equal to root-mean-square sound speed. Cold colors correspond to low sound speed (minimum of ~1440 m/s); warm colors reflect higher sound speed (maximum of ~1530 m/s); boundary between blue and yellow is 1505 m/s. A plot of SST measured during the seismic survey is superimposed; the front between the LC and NAC is visible as an abrupt ~5°C increase in temperature at CMP 69500.

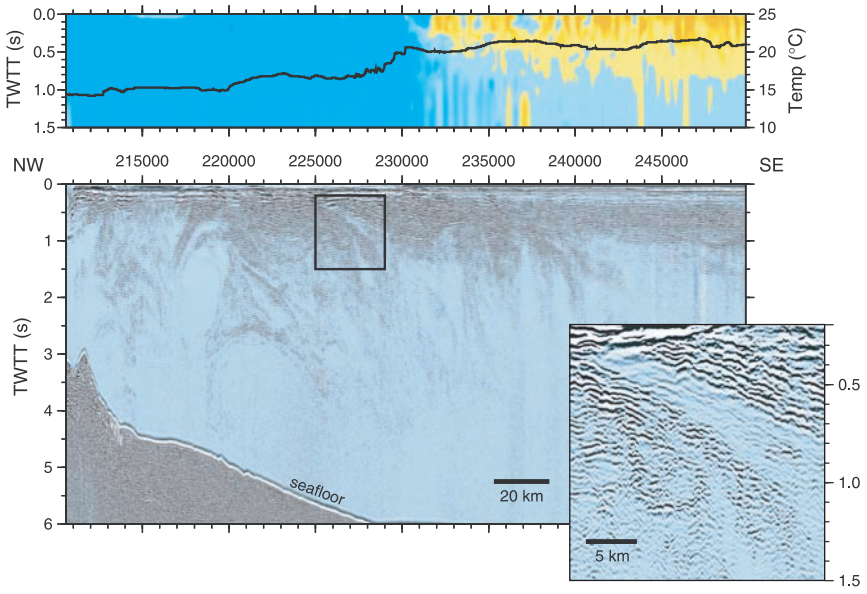

Fig. 3. Bottom: Stacked seismic section of water column on Line 2mcs, plotted as in Fig. 2, except with a vertical exaggeration of 27. Box denotes portion of profile depicted in inset, which shows "slabs" losing coherency at depths of ~1000 m. Top: Stacking sound speed and SST, plotted as in Fig. 2. The front is visible at CMP 229000.

intrusions, and the observed reflectance shows remarkable agreement with previously observed 20- to 30-m vertical-scale fine structure at this major front. On all three transects, the strongest reflectance occurs on the warm-water side of the warm/cold front (Figs. 2 to 4). The east-dipping reflections appear to outcrop at the sea surface in regions of locally low and/or variable SSTs. The eastward dip of reflections at the main front matches the expected inclination of density surfaces embedded within thermohaline intrusions caused by double-diffusive processes where warm water (NAC) lies above and to the east of colder water (LC) (*21*). Individual reflective layers are 20 to 30 m thick, are continuous for up to 10 km, dip down to the east at about 1°, and have reflection coefficients of 0.0004 to 0.003, corresponding to sound speed contrasts of 1 to 10 m/s.

West of the temperature front, long, continuous reflections dominate the uppermost ocean. On Line 1mcs, individual reflections dip gently (~0.3°) down to the east and can be traced continuously for up to 30 km over a zone about 100 km wide and 400 m thick. On Lines 2mcs and 3mcs, reflections in this zone form concave-upward "bowls" ~400 m thick and 40 to 50 km wide. Reflections here are the strongest anywhere on the transects, with reflection coefficients up to 0.005, corresponding to sound speed changes of about 15 m/s.

Beneath the frontal wedge and the zone of long continuous reflections, coherent, reflective slabs are common. These slabs are typically 100 to 300 m thick, dip at 1° to 4°, and reach down to about 1.5 s (~1100 m). In their upper reaches, the slabs contain laterally continuous reflections with reflection coefficients of 0.002, corresponding to sound speed contrasts of 6 m/s. These reflections strongly resemble, in both character and amplitude, those in the lower parts of the "wedge" that occupies the uppermost 400 m of the ocean at the front. At greater depths, the slabs' internal reflectance becomes progressively weaker (down to reflection coefficients of 0.0002) and more discontinuous, and by about 1000 m depth, the slabs largely lose their identity. These characteristics suggest that the slabs represent bands of strong temperature gradients, perhaps comprising contrasting waters that intrude along isopycnals and become progressively homogenized by mixing with surrounding waters. The dominantly eastward dip of the slabs mimics the shape of isopycnals measured in April 1980, which deepen by about 800 m across the front (*16*), although the 1980 station spacing was too coarse to reveal the tilting structures that we believe represent nearly isopycnal intrusions in the front. Nearby tow-yo data (*15*) show strong intrusions at vertical and horizontal scales that match the structures imaged here in the upper ocean; our images suggest that such features likely exist at greater depths than sampled by the tow-yos.

The deeper ocean (beneath 1000 m) is generally less reflective than the upper ocean, but important exceptions occur. West of the front on Line 2mcs, domed structures at a depth of 2.4 s (1800 m) are suggestive of subthermocline eddies previously reported in this region (*22*). In the area where slabs occur in the upper 1.5 s, there are measurable reflective structures down to about 4 s (3000 m). Indeed, in some instances, weakly reflective zones can be traced down from the base of a coherent slab to depths of 3 to 4 s (2250 to 3000 m). Individual reflectors within the structures tend to be oriented more horizontally than the reflective band itself. Because large-scale subduction of particular water types is unlikely during the stable stratification of this summer cruise, we speculate that these features indicate the boundaries of subthermocline eddies, possibly with intrusive fine structure spiraling around the eddy. Weak thermohaline intrusions should be possible on the boundaries of the Labrador Sea Water eddies reported in these regions (*22*). Deeper in the section, weak bands of horizontal reflections occur down to about 4.0 s

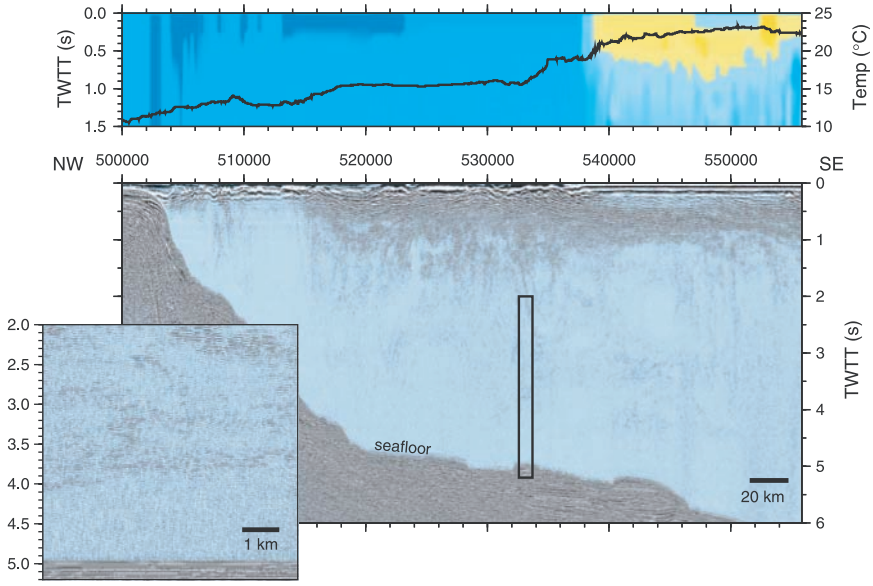

Fig. 4. Bottom: Stacked seismic section of water column on Line 3mcs, plotted as in Fig. 2, except with a vertical exaggeration of 39. Box denotes portion of profile depicted in inset, which shows horizontal reflections in deep water overlying a transparent zone of bottom water, which we speculate corresponds to Norwegian-Greenland Overflow Water. Top: Stacking sound speed and SST, plotted as in Fig. 2. The front is visible at CMP 535000.

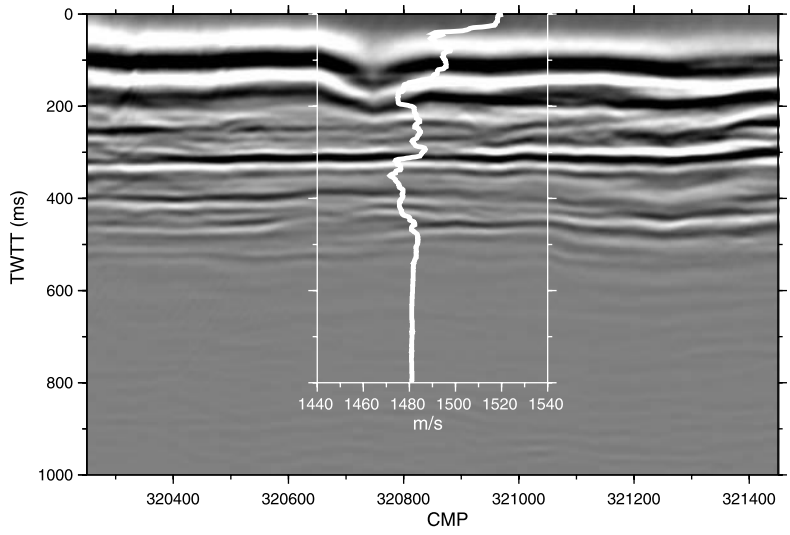

Fig. 5. Stacked seismic section on portion of Line 303 (Fig. 1), showing detail of reflections. White line shows sound speed structure calculated from temperatures recorded on an XBT located at CMP 320850. Note the excellent correspondence of reflectance in the upper 0.5 s (375 m) to fine-scale temperature variations.

(~3000 m depth), below which abyssal waters are devoid of detectable reflections (Fig. 4). Because this feature is consistent in the sections, we speculate that the transition from reflective to transparent waters at ~3000 m depth may represent the boundary between Labrador Sea Water and Norwegian-Greenland Overflow Water of the Deep Western Boundary Current (*22, 23*).

The ability to create detailed images of thermohaline structure in the ocean with low-frequency marine seismic reflection techniques adds a promising new tool for studies of oceanographic processes. The structures imaged in our North Atlantic transects have important implications for oceanic mixing and exchange processes and raise the possibility that the boundaries of deep water masses such as North Atlantic Bottom Water can be mapped seismically. Low-frequency seismic reflection techniques appear well-tuned to image thermohaline fine structure, provided that layers are at least 5 m thick and laterally continuous over hundreds of meters. Reflection techniques offer several advantages—including enhanced lateral resolution (trace spacing of ~6 m), the ability to simultaneously image large sections of the ocean, and opportunities for three-dimensional and time-lapse imaging—that make them an ideal complement to more traditional methods of probing the ocean, which are more limited in their space-time resolution. Finally, our results imply that the extensive global archive of marine seismic reflection data constitutes a large, untapped resource for probing ocean structure.

References and Notes

1. H. Stommel, K. N. Federov, *Tellus* **19**, 306 (1967).
2. R. D. Pingree, *Deep Sea Res.* **16**, 275 (1969).
3. R. W. Schmitt, H. Perkins, J. D. Boyd, M. C. Stalcup, *Deep Sea Res.* **34**, 1655 (1987).
4. T. M. Joyce, *Deep Sea Res.* **23**, 1175 (1976).
5. T. M. Joyce, *J. Phys. Oceanogr.* **7**, 626 (1977).
6. T. M. Joyce, W. Zenk, J. M. Toole, *J. Geophys. Res.* **83**, 6093 (1978).
7. D. Rudnick, R. Ferrari, *Science* **283**, 526 (1999).
8. J. Gonella, D. Michon, *C. R. Acad. Sci. Paris Ser. II* **306**, 781 (1988).
9. J. D. Phillips, D. F. Dean, in *Ocean Variability and Acoustic Propagation*, J. Potter, A. Warn-Varnas, Eds. (Kluwer Academic, Dordrecht, Netherlands, 1991), pp. 199–214.
10. L. R. Haury, M. G. Briscoe, M. H. Orr, *Nature* **278**, 312 (1979).
11. P. H. Wiebe, T. K. Stanton, M. C. Benfield, D. G. Mountain, C. H. Greene, *IEEE J. Ocean. Eng.* **22**, 445 (1997).
12. The observed reflections are coherent in both the shot and CMP domains, and thus cannot be seafloor multiples from previous shots, which are coherent only in the shot domain.
13. We have not applied migration (a process that places dipping events in their proper spatial position) to the images shown. However, because of the small dips of reflectors, migration does not change the images appreciably. We show unmigrated sections because migration artifacts from the seafloor reflection, which has a much higher amplitude than the water column reflections, degrades the deeper portions of migrated sections.
14. The sound source was a 140-liter, 20-element airgun array, and reflections were recorded on a 480-channel, 6-km-long hydrophone streamer. Data were digitized at a sample interval of 4 ms and have a frequency content of 10 to 100 Hz, with a peak frequency near 40 Hz.
15. R. W. Schmitt, D. T. Georgi, *J. Mar. Res.* **40** (suppl.), 659 (1982).
16. D. T. Georgi, R. W. Schmitt, *J. Phys. Oceanogr.* **13**, 632 (1983).
17. Using data corrected for spherical divergence, we calculated the reflection coefficient of the seafloor as $-A_{mult}/A_{sf}$, where A_{mult} is the amplitude of the first seafloor multiple and A_{sf} is the amplitude of the seafloor reflection (*18*). We then calculated reflection coefficients in the water column from the ratio of the amplitudes of water column reflections and the seafloor reflection.
18. M. Warner, *Tectonophysics* **173**, 15 (1990).
19. C. Garrett, W. Munk, *Annu. Rev. Fluid Mech.* **11**, 339 (1979).
20. Because the profiles are collected by a ship traveling at a rate of about 8 km/hour, the images can only be regarded as instantaneous "snapshots" at local scales of about 2 km.
21. B. Ruddick, K. Richards, *Prog. Oceanogr.* **56**, 499 (2003).
22. R. S. Pickart, W. M. Smethie, J. R. N. Lazier, E. P. Jones, W. J. Jenkins, *J. Geophys. Res.* **101**, 20711 (1996).
23. R. S. Pickart, *Deep Sea Res.* **29**, 1553 (1992).
24. P. Wessel, W. H. F. Smith, *Eos* **72**, 441 (1991).

25. We thank the captain and crew of the R/V *Maurice Ewing* for a successful cruise, and A. Gorman, D. Lizarralde, J. Stennett, K. Polzin, T. Joyce, E. Montgomery, and D. Shillington for helpful conversations. B. Tucholke, K. Louden, J. Hopper, H. C. Larsen, and H. van Avendonk contributed to data acquisition. Data were processed using Sioseis, Paradigm's Focus software, and Generic Mapping Tools (*24*). Supported by NSF grants OCE-9819599 (W.S.H.) and OCE-0081502 (R.W.S.).

31 March 2003; accepted 29 May 2003

Observation of Long Supershear Rupture During the Magnitude 8.1 Kunlunshan Earthquake

Michel Bouchon* and Martin Vallée

The 2001 Kunlunshan earthquake was an extraordinary event that produced a 400-km-long surface rupture. Regional broadband recordings of this event provide an opportunity to accurately observe the speed at which a fault ruptures during an earthquake, which has important implications for seismic risk and for understanding earthquake physics. We determined that rupture propagated on the 400-km-long fault at an average speed of 3.7 to 3.9 km/s, which exceeds the shear velocity of the brittle part of the crust. Rupture started at sub–Rayleigh wave velocity and became supershear, probably approaching 5 km/s, after about 100 km of propagation.

The Kunlunshan earthquake that hit Tibet on 14 November 2001 produced the longest rupture yet observed for an earthquake on land. The mapped surface break of the earthquake extends for ~400 km (*1*, *2*). The exceptional length of this event and the presence of several regional broadband stations of the China Digital Seismic and Incorporated Research Institutions for Seismology (IRIS) networks provide a unique opportunity to determine the speed at which rupture propagates on a fault during an earthquake. In the past, it has been thought that earthquake rupture can only propagate at speeds below the Rayleigh-wave velocity of crustal rocks, which, at about 0.92 times the shear (*S*)–wave velocity, lies in the range of 3.0 to 3.2 km/s for the brittle part of the crust. This belief was backed by fracture dynamics theory, which shows that a rupture cannot propagate at a speed between the Rayleigh-wave and *S*-wave velocities. However, more recent works (*3*–*5*) show that, although the range of velocity between the Rayleigh and *S* waves is not allowed, shear cracks can theoretically propagate at intersonic speeds; that is, at speeds between the *S*-wave and the pressure (*P*)–wave velocities. Subsequent theoretical (*6*–*8*) and experimental (*9*, *10*) studies in fracture dynamics confirm these findings.

Values of rupture velocity inferred from studies of earthquakes support the Rayleigh velocity limit to earthquake rupture with a few exceptions of reported observations of supershear rupture (*11*–*15*). Although these observations have not been fully accepted, they have nevertheless generated strong interest in understanding conditions that can lead to supershear rupture (*16*, *17*) and in assessing its seismic risk consequences (*18*).

The Kunlunshan earthquake was recorded in Tibet and surrounding regions by broadband seismic stations (fig. S1). These stations lie at distances between 600 and 1900 km from the fault, a distance range at which the records are dominated by surface (Rayleigh and Love) waves and, especially, because of the strike-slip mechanism of the

Université Joseph Fourier and Centre National de la Recherche Scientifique, Laboratoire de Géophysique Interne et Tectonophysique, Boîte postale 53, 38041 Grenoble, France.

*To whom correspondence should be addressed. E-mail: Michel.Bouchon@ujf-grenoble.fr